# Effects of Planetesimal-Scale Evaporation on Pb Isotopic Evolution and Timing of the Last U/Pb Fractionation

**Tong Fang[1,*], Wei-dong Sun[1-3], and Robert E. Zartman[1]**

[1]Center of Deep Sea Research, Institute of Oceanology, Center for Ocean Mega-Science, Chinese Academy of Sciences, Qingdao 266071, China

[2] Laboratory for Marine Mineral Resources, Qingdao National Laboratory for Marine Science and Technology, Qingdao 266237, China

[3] University of Chinese Academy of Sciences, Beijing 100049, China

[*] Corresponding author: Tong Fang (fangtong2019@qdio.ac.cn)

**Key Points:**

- The collisional evaporation within the first 20% accretion causes 80%-90% Pb loss of the proto-Earth
- The early planetesimal-scale evaporation of Pb postpones the timing of the last U/Pb fractionation
- The early evaporation combined with the late fractionation driven by the segregation of the "Hadean matte" likely explains the Pb paradox

## Abstract

The excess of radiogenic lead (Pb) isotopes in the silicate Earth, which is referred to as “the first terrestrial Pb paradox” has remained a confusion for a long time. A large-scale U/Pb fractionation with an increase of μ value ($^{238}U/^{204}Pb$) compared with CI chondrite is proposed to be the main culprit. The volatile e.g., Pb diffuses into space from the planetesimal-scale collisional melting, which plays a critical role in Pb loss on the accreting proto-Earth. The N-body simulation describes the collisional history of terrestrial planets in the first 200 million years of the Solar System. The collisional information provides the degree of silicate melting and further obtains the volatile loss fraction. Within the early 20% accretion of proto-Earth, the cumulative fraction of Pb loss can reach 80%-90%. Meanwhile, the μ value could rise to 1.5-4 setting the initial value to be 0.2-0.6. Besides, the silicate melting with higher temperature and lower oxygen fugacity (relatively reduced condition) can bring about more Pb loss. Further increase of μ to 9.26 possibly caused by a late large-scale U/Pb fractionation can effectively explain the excess of radiogenic Pb isotopes in the bulk silicate Earth. The two-stage model with the planetesimal-scale evaporation predicts a young age of 240 million years of the last large-scale fractionation event. The last fractionation is more consistent with the “Hadean matte” event than a late Moon-forming giant impact.



## Plain Language Summary

Pb as a volatile element is easily lost to space through evaporation in high-temperature events during the early growth of Earth. We simulate the Earth’s growth and estimate how large a fraction of Pb is lost to space. Pb can also be replenished through the decay of uranium. We find that the early evaporation cannot explain the current U/Pb ratio and the isotopic composition of Pb. A late large-scale Pb loss is necessary to match the present-day value and this loss is likely caused by the

hidden reservoir called “Hadean matte” instead of the Moon-forming giant impact.

**Keywords:**

Lead paradox, Lead evaporation, N-body simulation, Collisional melting, Hadean matte

## 1. Introduction

Two uranium-lead (U-Pb) decay groups, $^{238}U$-$^{206}Pb$ ($\lambda=1.55125\times10^{-10}$ $year^{-1}$) and $^{235}U$-$^{207}Pb$ ($\lambda=9.8485\times10^{-10}$ $year^{-1}$), are widely applied to geological dating and researches of terrestrial Pb isotope evolution (Connelly et al., 2017). The evolution of U-Pb system in the bulk silicate Earth (BSE) depends on the early accretion and the subsequent magmatic processes (Murphy et al., 2003; Malaviarachchi et al., 2008; Albarède et al., 2009; Wood & Halliday, 2010; Burton et al., 2012). These processes result in a series of elemental fractionation between U and Pb for their individual geochemical characteristic (Malavergne et al., 2007; Bouhifd et al., 2013; Albarède et al., 2015). The ratios of radiogenic Pb isotopes to the stable $^{204}Pb$ ($^{206}Pb/^{204}Pb$ and $^{207}Pb/^{204}Pb$) are elevated with the decay time and their accumulation rates vary as $^{238}U/^{204}Pb$, termed as μ, changes (Connelly & Bizzarro, 2016). Notability, the Pb isotopic composition in the BSE samples generally plots to the right of the Earth isochron, which is referred to as “the first terrestrial Pb-isotope paradox” (Murphy et al., 2003; Hofmann, 2007; Connelly & Bizzarro, 2016).

The genesis of the Pb paradox is Pb loss from the Earth mantle and an increase of μ. The major part of Pb loss is attributed to the early Earth accretion (Connelly & Bizzarro, 2016). The lowest value of μ in the initial solar nebula is 0.27, according to the observation data of the solar photosphere (Anders & Grevesse, 1989). In the first few million years, the tiny gas and dust of the solar nebula condensed into small bodies; then they proliferated into small undifferentiated planetesimals (Norman & Mittlefehldt, 2002; Chambers, 2004). The formation of large planetesimals (<1000 km) and planet embryos (thousands of km) derives from high-energy collisions (Williams & Cieza, 2011; Elkins-Tanton, 2012). During these periods, Pb is constantly lost in the high-temperature evaporation events and μ increases, for Pb has a much lower 50% condensation

64 temperature (50% $T_C$) than U (Lodders, 2003; Wood et al., 2019). Besides, Pb can enter the metal
65 phase or dive into the metal core as the form of sulfide or iron alloy in the stage of core formation,
66 for Pb is a chalcophile element and has iron affinity under high pressure (Hart & Gaetni, 2006; Wood
67 & Halliday, 2010; Wood et al., 2010; Burton et al., 2012; Ballhaus et al., 2013). As a result, the μ
68 value in the silicate part of terrestrial planets e.g., Earth increases episodically during the early
69 accretion.

70 Some evidence suggests that volatility dominants the Pb loss rather than the iron affinity
71 (Albarède et al., 2015; Connelly & Bizzarro, 2016). For example, the contents of chalcophile and
72 moderately volatile elements (like Zn, Cu, Rb, Pb, Tl, etc.) are related to their bond energy strength
73 (Albarède et al., 2015). Besides, the composition of siderophile elements strongly deviates from the
74 volatility trend line compared with other chalcophile and moderately volatile elements, including Pb
75 (Palme & O'Neill, 2014). The evaporation of the melting rocks caused by violent collisions occurs on
76 planetesimals of a few to hundreds of kilometers size (Young, 2017; Davies et al., 2020). It affects
77 the composition of elements and their isotopes, e.g., for major elements (Mg and Si) (Hin et al., 2017;
78 Young et al., 2019) and chalcophile moderately volatile elements (Ge, Zn and In) (Young, 2017).
79 Two types of vapor loss are proposed. One is the impact-induced evaporation and the other is the
80 direct outflow released from magma ocean or magma pool (Dauphas et al., 2015; Hin et al., 2017).
81 However, for large bodies, the high escape velocity needed makes it difficult for vapor to overcome
82 gravity and diffuse into space. Therefore, vapor loss is only effective for objects with masses less
83 than 0.2 $M_e$ (Earth mass) (Hin et al., 2017; Benedift et al., 2020). A cluster of planetesimals that
84 experience different times of collisions and multiple thermal evaporation events could have diverse
85 volatile composition. The terrestrial planets like Earth and Mars inherit the characteristic of

86 planetesimals with varying degrees of volatile depletion during numerous fractionation processes
87 (Sossi et al., 2019).

88 Pb is a moderately volatile element and it has a low 50% $T_C$ in the form of iron alloy and sulfide
89 (PbS) (Lodders, 2003; Wood et al., 2019). Pb is easily volatilized as sulfides and lost with silicate
90 vapor under high-temperature conditions (Wood & Wade, 2013; Sossi et al., 2019). The
91 planetesimal-scale evaporation driven by impacts causes a huge amount of Pb loss (Norris & Wood,
92 2017). As a result, Pb is comparatively depleted in the bulk silicate Earth relative to CI chondrites.
93 The content of Pb in BSE is only 0.07 times of that in CI chondrites (Palme & O'Neill, 2014). The
94 partition of Pb in the silicate vapor loss is decided by the temperature and oxygen fugacity of silicate
95 melt and it could be extremely high under the formation condition of magma ocean (Elkins-Tanton,
96 2012; Norris & Wood, 2017). As a result, the planetesimal-scale evaporation of Pb is thought to be a
97 critical factor for the increase of μ and the excess of radiogenic Pb isotope (Connelly & Bizzarro,
98 2016).

99 It is complex to obtain the cumulative Pb loss on the accreted planets. First, we need a model to
100 simulate the collisional process between planetesimals. The melting degree produced by each
101 collision is estimated with the collisional parameters. Subsequently, we need to calculate the fraction
102 of Pb loss under different temperatures and redox states of the melting pools. The purpose of this
103 study is to find out how the Pb loss caused by planetesimal-scale evaporation in the early accretion
104 contributes to the variation of U/Pb ratio and Pb isotopic composition of the bulk silicate Earth.

105 **2. Numerical Methods**

106 The terrestrial planets form from the collisions and merge between planetesimals and planet
107 embryos. This process can be restored by the N-body collisional accretion simulation (Chambers,

1999; Hansen, 2009; Fischer & Ciesla, 2014; Carter et al., 2015; Fang & Deng, 2020). We use the Mercury6 package (Chambers, 1999) and the same initial conditions as Hansen (2009), setting a uniform areal density within a narrow annulus from 0.7 to 1 AU. The annulus is sampled with 400 planetesimals of the equal mass, 0.005 $M_e$ (that is 0.005 times the Earth mass). Through N-body simulation, three or four large planet bodies can be formed in the inner planetary disk, which are prototypes of terrestrial planets (Fang & Deng, 2020). N-body simulations roughly restore the evolutional history of these analogues within the first 200 million years (Myr). The Earth analogue completes mass growth within 50-160 Myr from the initial planetesimal of 0.005 $M_e$ according to 100 groups of simulations. The first 20% mass accretion of the Earth, from 0.005 $M_e$ to 0.2 $M_e$, is completed within 3 Myr. The output of each simulation gives the times of collisions, the masses of impactors and targets, and the velocities and angles of collisions. Based on these parameters, the melt volume and depth induced by a collision can be calculated, as well as the vapor loss (de Vries et al., 2016; Hin et al., 2017).

The collisions between planetesimals or collisions between planetesimal and planet embryo produce shock melting on the targets. The melting volume and depth induced by the high-energy impact are proportional to the shock energy of projectiles (Barr & Citron, 2011). The shock energy depends on the mass and velocity of the projectile, the impact angle, and the composition of the target which determines the internal energy generated under impact pressure (Barr & Citron, 2011; Abramov et al., 2012; de Vries et al., 2016). Based on the dimensional analysis model of Bjorkman and Holsapple (1987), the melt volume is expressed as $V_{melt} = 0.22E_m^{-0.85}(\rho_p/\rho_t)D_p^3v^{1.7}\sin^{1.3}\theta$, where $\rho_p$ and $\rho_t$ represent the density of the projectile and target, respectively. $D_p$ is the diameter of the projectile. $E_m$ represents the special energy of melting as the Rankine-Hugoniot state (Bjorkman

130 & Holsapple, 1987) and it changes with temperature. The energy required for melting decreases
131 when the temperature of the target increases. This formula is widely used in previous studies
132 (Abramov et al., 2012; de Vries et al., 2016; Davies et al., 2020). The result of the N-body simulation
133 provides the size of the projectile, impact velocity, and angle. Each simulation assumes an identical
134 density for the projectile and target (3000 kg/m$^3$) so that the mass and volume of collisional melting
135 can be calculated via the above formula. Assuming the initial melt is roughly spherical, the average
136 melting radius is $R_m = (3V_m/4\pi)^{1/3}$ (Abramov et al., 2012).

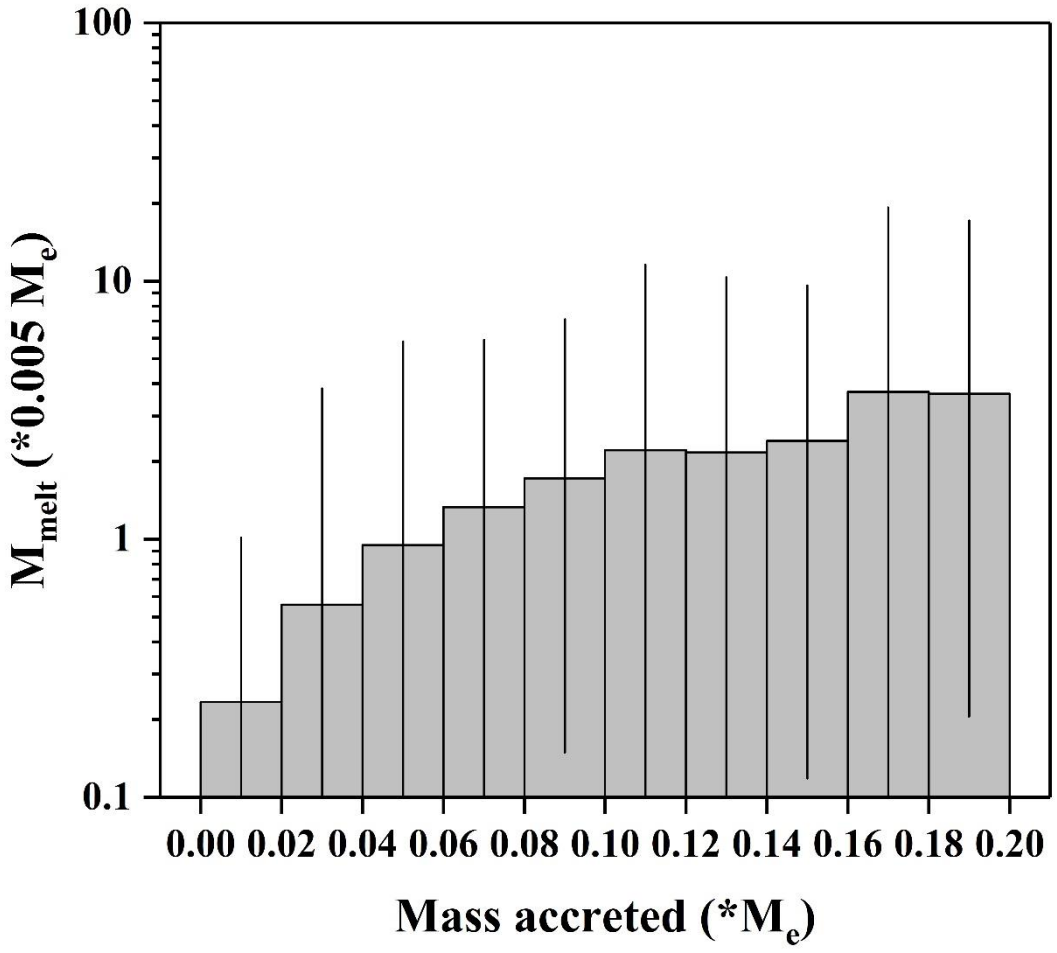


137

138 **Figure 1.** The average melting mass ($M_{melt}$) driven by multiple collisions evolves with the accreted
139 mass of the targets. Data of collisional melting derives from 100 groups of N-body simulations and
140 the error bars represent the maximum and minimum of the melting mass.

From the above formula of collisional melting, the generated melt volume has a positive correlation with the diameter of the projectile and collisional velocity (Abramov et al., 2012; de Vries et al., 2016). When the collisional angle is closer to vertical, more collisional energy is produced by the impact. The statistics of 100 sets of simulations indicate that a single collision generally produces silicate melting with less than 60% mass of the target during the first 20% accretion (Figure 1). The melting depth ranges from 500 km to 3000 km. In the early stage of the Earth accretion, frequent but small-scale collisions produce minor melt. While the melting intensifies with time and accreting mass (Figure 1). The increase of melting mass results in a huge amount of silicate vapor loss with volatiles escaping into space.

## 3. The Variation of the μ Value

The ratio of U/Pb is expressed as μ ($^{238}U/^{204}Pb$). The value of μ is controlled by the fractionation of U and Pb in the geological process. U and Pb have very different geochemical properties. U is a refractory lithophile element and it easily concentrates in the initial planetesimals. Pb is a moderately volatile and chalcophile element. It volatilizes during the accretion process or possibly enters the metal core as sulfides during the core formation. In these processes, the μ value of the silicate part continuously increases. The geological bodies with larger μ value further concentrate more radiogenic Pb isotopes.

### 3.1. The μ values in the planetary bodies

As shown in Table 1, the μ value of CI chondrites is around 0.2-0.22 (Palme & O'Neill, 2014; Carlson et a., 2015) and it is the minimum value among planetary bodies. Because the CI chondrites have a similar elemental distribution with the initial solar nebula, its μ value can primely represent the μ value of the earliest undifferentiated bodies (Scott, 2007; Albarède, 2009). The μ value of the

163 solar photosphere is 0.27 close to the initial value (Anders & Grevesse, 1989). In the accreted
164 systems, the μ value is higher than 0.22. For example, other carbonaceous chondrites show μ values
165 in the range of 0.30-0.62 (Newsom et al., 1995). The previous research measured the μ value of the
166 L3 ordinary chondrite to be 1.8 (Connelly & Bizzarro, 2016). The protoplanets which experience
167 multi-stage U/Pb fractionation show a much higher μ value than the undifferentiated bodies. By
168 measuring different types of Martian meteorites, the range of the Martian mantle's μ value is from
169 1.5 to 5 with a medium value of 3 (Bouvier et al., 2005; Gaffney et al., 2007; Bouvier et al., 2009;
170 Yoshizaki & McDonough, 2020). Martian mantle is less depleted in the volatiles and it shows a
171 lower μ value than the Earth and Moon (Allègre et al., 1995; Premo et al., 1999). The measured μ
172 value of modern bulk silicate Earth is in the range of 8-10 with an average value of 9 (Allègre et al.,
173 1995; McDonough & Sun, 1995; Palme & O'Neill, 2014). Therefore, samples of modern BSE have
174 generally enriched in radiogenic Pb isotopes and their μ value is much higher than that of the original
175 material in the Solar System (Galimov, 2011, 2019).

176 **Table 1**

177 *The μ value in planetary reservoirs*

| Planetary reservoirs | $\mu(^{238}U/^{204}Pb)$ | References |
|---|---|---|
| Solar Photosphere | 0.27 | (Anders & Grevesse, 1989) |
| CI chondrites | 0.22 | (Carlson et al., 2015) |
| CM chondrites | 0.33 | (Newsom et al., 1995) |

| | | |
|---|---|---|
| CO chondrites | 0.30 | (Newsom et al., 1995) |
| CV chondrites | 0.62 | (Newsom et al., 1995) |
| L3 ordinary chondrite | 1.8 | (Connelly & Bizzarro, 2016) |
| Bulk silicate Mars (BSM) | 1.5-5 | (Gaffney et al., 2007) |
| Bulk silicate Earth (BSE) | 8-10 | (McDonough & Sun, 1995) |

### 3.2. The upper limit of the cumulative Pb loss

The amount of Pb loss driven by collisional evaporation on planetesimals is decided by the collisional melting degree as well as the partition of Pb between the gas phase and melt phase. The former can be calculated from the results of the N-body simulations. The distribution of volatile elements in melt and vapor is controlled by temperature, oxygen fugacity, and volatile species (Wood & Wade, 2013; Norris & Wood, 2017). Pb is moderately volatile and easily evaporate as sulfides (the 50% $T_C$ of PbS is 495 K) (Wood et al., 2019). In the silicate melt, Pb can also volatilize in the form of PbO under high temperatures (Wood & Wade, 2013; Sossi et al., 2019). When the temperature rises above 1400℃ and the logarithm of the oxygen fugacity ($\log fO_2$) is below -10, almost all Pb in silicate melt volatilizes as PbO or Pb (Sossi et al., 2019).

Pb is more concentrated in sulfides compared with silicate minerals ($D_{\text{sulfide/silicate mineral}}$=5-2000 and $D_{\text{sulfide/peridotite}}$=114.4) (Burton et al., 2012). The initial content of sulfur before accretion is around 5.35% according to CI chondrite, much higher than that of modern BSE (0.02%) (Palme & O'Neill,

192 2014). Therefore, the total Pb content in the sulfide is several times that in the silicate at the
193 beginning of accretion and it decreases as the sulfur is lost. We assume that the sulfur content
194 decreases linearly with accreting mass.

195 Assuming that all Pb in the melting pool volatilizes as PbS, PbO, and Pb and no Pb enter the
196 core, we obtain the largest degree of Pb loss (T>1400℃ and log$fO_2$<-10). Figure 2 shows the
197 cumulative Pb loss fraction and Pb loss fraction in sulfide and silicate respectively within the first 20%
198 accretion. With reference to the results of all simulations, the cumulative Pb loss accounts for more
199 than 75% of the initial Pb content, mostly around 80%-90% when the Earth-mass accretes from
200 0.005 $M_e$ to 0.2 $M_e$. The continuous loss of S during the first 20% accretion results in a decrease of
201 the proportion of Pb loss as sulfide relative to the entire Pb loss, that is, the height of blue bars in
202 Figure 2 decreases.

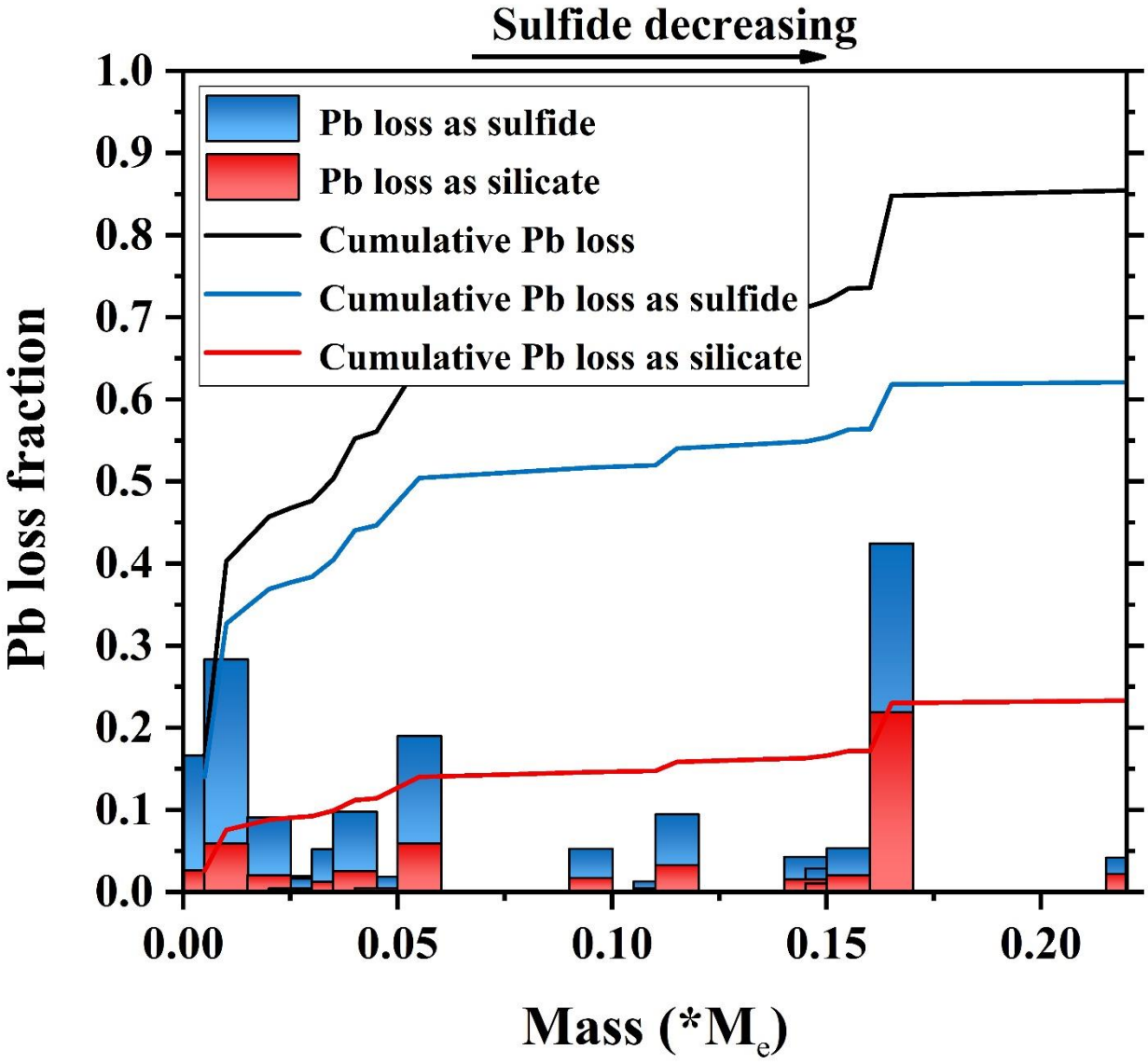


**Figure 2.** Pb loss fraction for each impact (bars) and the cumulative Pb loss fraction (curves) in one N-body simulation until the accreted mass is up to 0.2 $M_e$. The blue bar and curve represent Pb loss as sulfides; the red bar and curve represent Pb loss as oxides in silicate; the black curve represents the sum of cumulative Pb loss in sulfide and silicate. The content of sulfur linearly decreases with the accreting mass during the first 20% accretion.

### 3.3. Increase of μ in the accreting planetesimal

The degree of increase of μ is directly related to the amount of Pb loss with a constant U content

in the multi-stage evaporation event. Under the extreme condition of the maximal Pb loss, the value of μ after the n*th* evaporation is expressed as $\mu_n = \mu_{n-1}/(1-F)$ ($F = M_{melt}/M_i$). When the magma ocean is relatively oxidized, the degree of Pb evaporation is limited by the temperature and oxygen fugacity (Wood & Wade, 2013; Norris & Wood, 2017). According to the Hertz-Knudsen-Langmuir (HKL) theory, researchers obtain the volatility factors of volatile species like Pb (Sossi et al., 2019). Pb directly evaporates to PbO(g) at high oxygen fugacity and decomposes to Pb(g) at low oxygen fugacity. The two reactions generally coexist. The partial pressure of PbO(g) and Pb(g) under different oxygen fugacity and temperature determines the residual fraction of PbO in the silicate melt: $f_{PbO}(melt) = \exp(-(K^*(PbO) + K^*(Pb)/fO_2^{1/2})\ 3/r\rho\ (M/2\pi RT)^{1/2}\ (t-t_0))$ (Sossi et al., 2019). The results of $f_{PbO}$(melt) are available under different oxygen fugacity at 1300℃ and 1400℃ respectively from the experimental data in Sossi et al. (2019). In this case, the value of μ after the n*th* evaporation can be expressed as $\mu_n = \mu_{n-1}/(R_{PbO} * f_{PbO}(melt) * F_n + (1-F_n))$. $R_{PbO}$ is the proportion of Pb in silicate and this value increases as sulfur content decreasing.

The planetesimal-scale Pb loss and μ increment happen in the first 3 Myr (the first 20% accretion). The earliest condensation in the solar nebula produces Moon-size small bodies within 1 Myr (Chamber, 2004; Johansen et al., 2007) and μ starts to grow in this stage from 0.22. The initial μ value of the undifferentiated planetesimals is larger than 0.22. Each collisional melting and evaporation are accompanied by a raising of μ value. We use an initial μ value in the range of 0.22-0.6 and find out that the μ value rises up to 1.5-5 in the first 20% of Earth accretion (Figure 3). In Figure 3, the temperature and oxygen fugacity have effects on the evolution of μ value. When T>1400℃ and log$fO_2$<-10, Pb in the melt is totally lost and the cumulative μ value could increase to

the highest level (Sossi et al., 2019). A decline of temperature or an increase of oxygen fugacity can both bring down the Pb loss fraction in the silicate melt, resulting in a lower cumulative μ value (Figure 3). As a result, a high-T and reduced condition contribute to a high μ value in the silicate Earth.

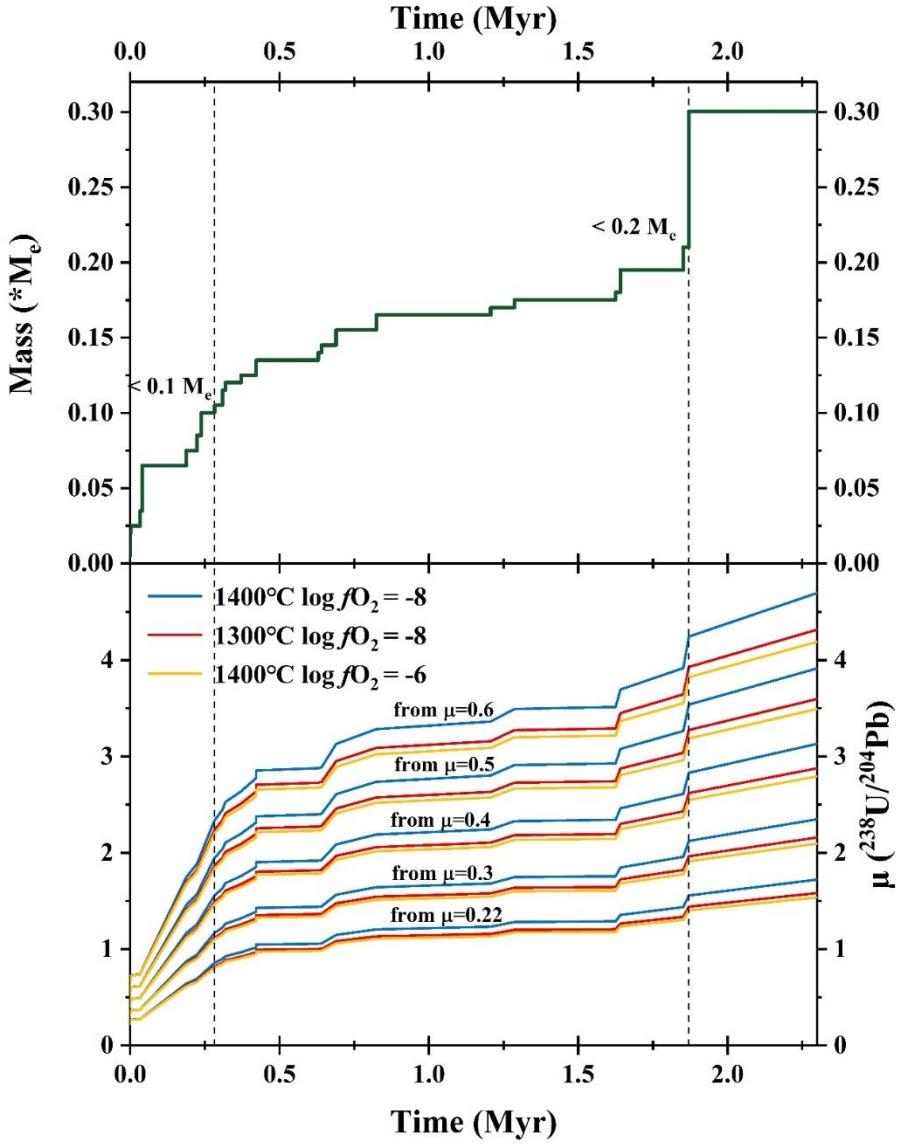


**Figure 3.** The accreted mass with time and the temporal evolution of the μ value during the first 20% accretion for one N-body simulation. The initial μ value is set to be 0.22-0.6 respectively. The blue curves show the variation of μ under 1400°C and log$fO_2$=-8; the red curves show the variation of μ under 1300°C and log$fO_2$=-8; the yellow curves show the variation of μ under 1400°C and log$fO_2$=-6.

### 3.4. An additional Pb loss in the late fractionation event

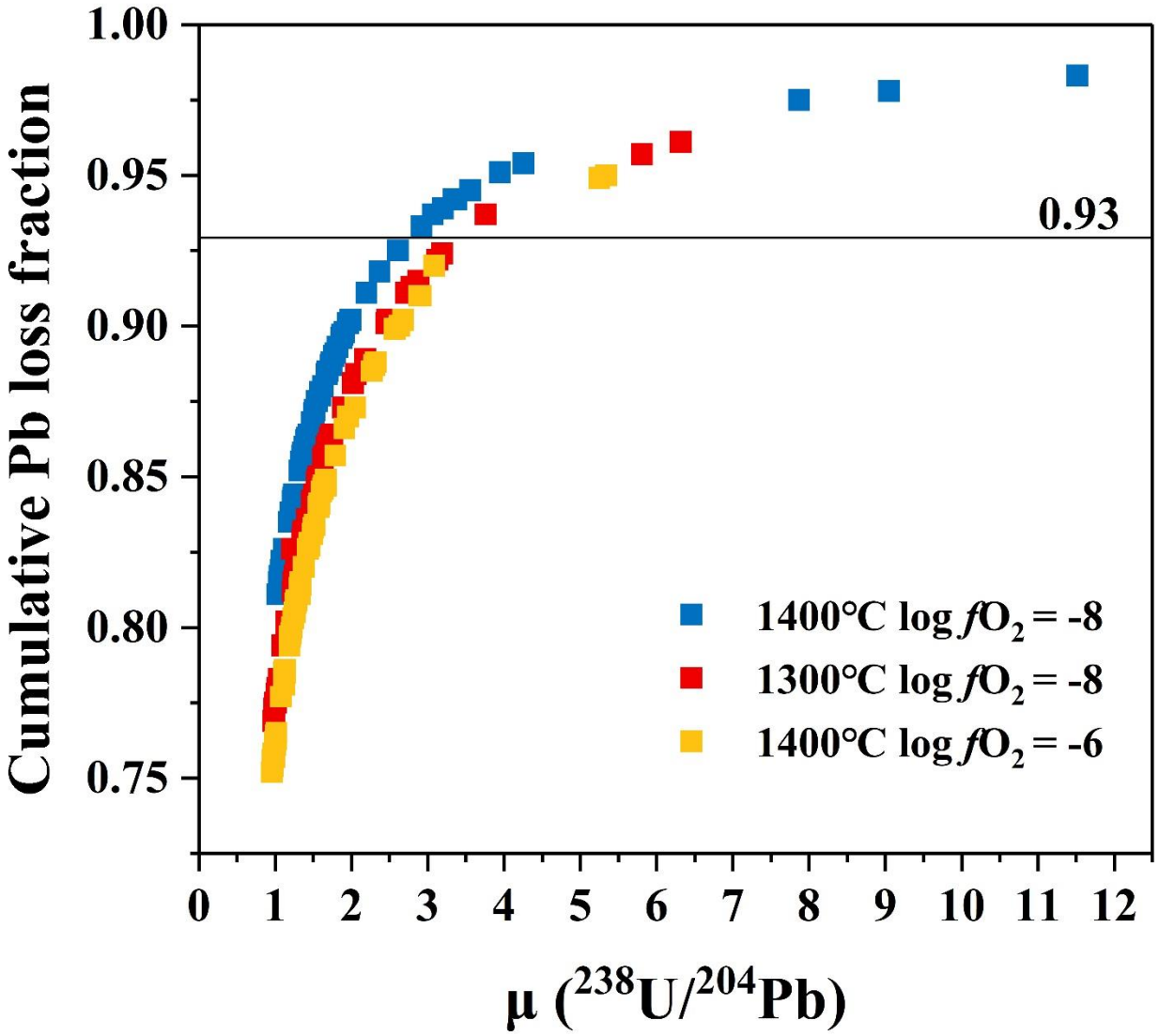


**Figure 4.** The relation of the μ value before the last U/Pb fractionation to the cumulative Pb loss fraction under three T-log$fO_2$ conditions. The results derive from 63 groups of N-body simulations. The current Pb loss fraction is estimated to be 0.93 (Palme & O'Neill, 2014).

There is at least 93% Pb loss from the proto-Earth according to the Pb content of CI chondrites and the primitive mantle in Palme and O'Neill (2014). However, in the planetesimal-scale evaporation model, the average fraction of Pb loss is around 84% and it cannot reach 93% in most cases (Figure 4). Meanwhile, the early evaporation hardly raises the μ value to the value of modern

BSE which is around 8-10 (Palme & O'Neill, 2014). Other events are proposed to explain the subsequent Pb loss, for example, Pb entering into the core in the stage of core formation, Pb evaporation in the last giant impact, or Pb missing with the iron sulfide melts (Hart & Gaetni, 2006; Wood & Halliday; 2010; Ballhaus et al., 2013; Savage et al., 2015; Connelly & Bizzarro, 2016; Maltese & Mezger, 2020).

Proto-Mars experiences rapid accretion and completes its core formation within the first 30 Myr (Elkins-Tanton, 2012). Mars is considered to be an original planet embryo that has not suffered a giant fractionation event (Elkins-Tanton, 2012). The μ value of the Martian mantle is in the range of 1.8-5 (Borg et al.2005; Gaffney et al., 2007), which is generally consistent with the post-evaporation μ value of the proto-Earth. This suggests that the subsequent μ increase is probably related to a late U/Pb fractionation event (Figure 5), e.g., the Moon-forming event (Canup & Asphaug, 2001; Deng et al., 2019). We estimate the effect of such a large-scale fractionation on the final μ value and Pb isotopic composition in the following sections.

## 4. The Necessity of a Late Fractionation from the Rb-Sr System

Rubidium (Rb) is a volatile lithophile element. The 50% $T_C$ of Rb as feldspar phase is about 750-800 K (Wood et al., 2019). Rb is easily lost in the high-T evaporation events and is extremely depleted in the Moon (Galimov, 2011, 2019). The early evaporation driven by collisional melting results in Rb loss and Pb loss at the same time. Therefore, the $^{87}Rb/^{86}Sr$ ratio, expressed as κ, decreases as μ increases. A previous study shows a generally anti-correlation between the κ ($^{87}Rb/^{86}Sr$) and μ ($^{238}U/^{204}Pb$) from samples of Earth, Martian, and lunar mantle because of the strong volatility of Rb and Pb (Gaffney et al., 2007).

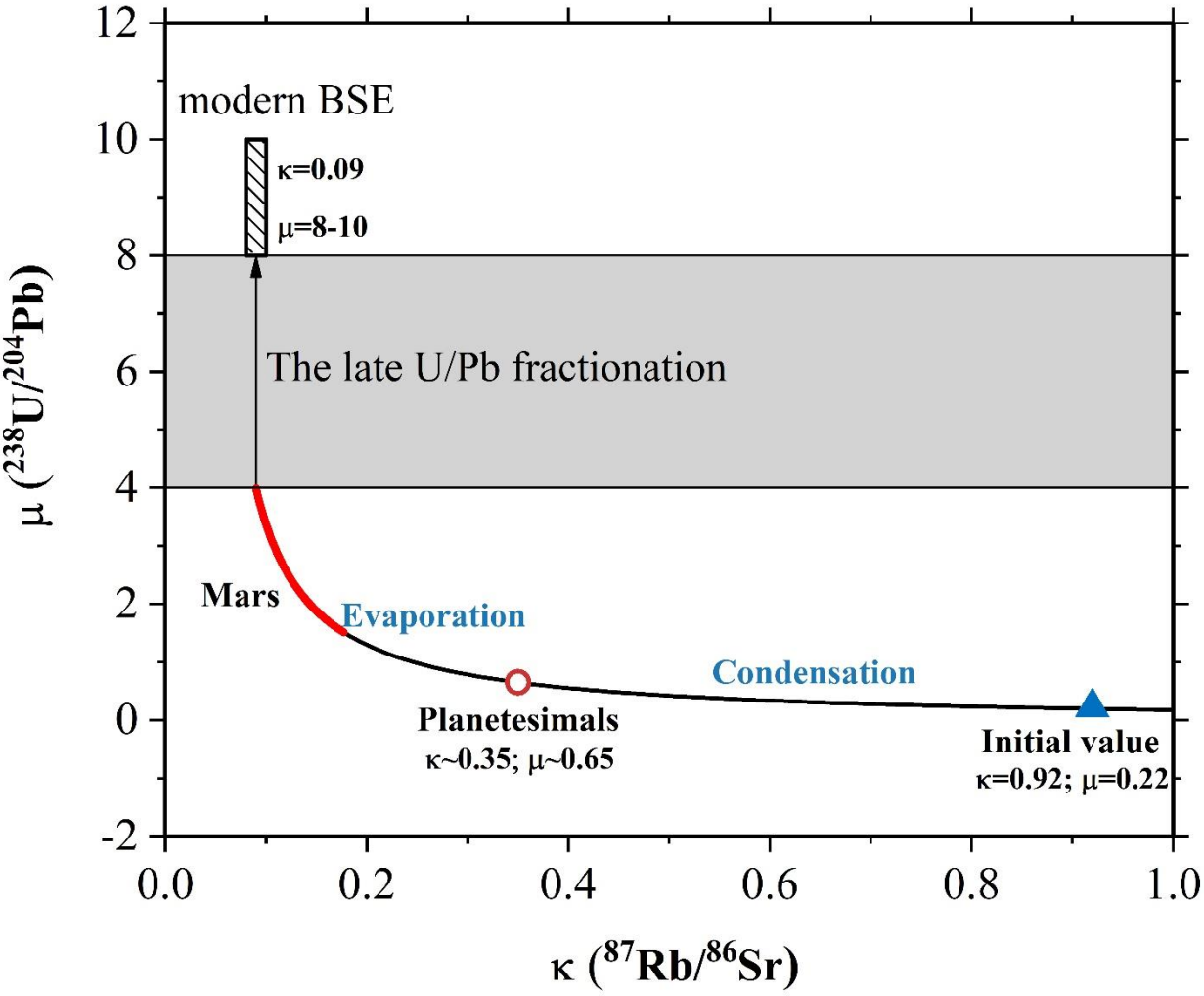


**Figure 5.** The relation of the variation of $\kappa(^{87}Rb/^{86}Sr)$ and $\mu(^{238}U/^{204}Pb)$ during the terrestrial accretion. The composition of CI chondrites represents the initial composition of the solar nebula ($\kappa$=0.92; $\mu$=0.22) (Palme & O'Neill, 2014). The condensation of nebula dust produces small undifferentiated bodies. The assumed value of planetesimals (0.005 $M_e$) is $\kappa$=0.35 and $\mu$=0.65 before evaporation. The accreted body like Mars shows $\kappa$ in the range of 0.12-0.26 and $\mu$ in the range of 1.5-5 (Gaffney et al., 2007; Yoshizaki & McDonough, 2020). The final $\kappa$ and $\mu$ values can approximately fall in the interval of the observed values of the present Earth mantle ($\kappa\approx$0.09; $\mu$=8-10) (Galimov, 2011). The additional increase of $\mu$ is caused by a late U/Pb fractionation.

Rb is less volatile than Pb and the volatility factor of Rb in the silicate melt is less than that of

Pb at the same temperature and oxygen fugacity (Sossi et al., 2019). The residual fractions in silicate melt for Pb and Rb satisfy (Sossi et al., 2019),$f_{Rb}(melt)/f_{Pb}(melt) = \exp(K^*(Rb)/fO_2^{1/4}M_{Rb}^{1/2})/\exp((K^*(PbO) + K^*(Pb)/fO_2^{1/2})M_{Pb}^{1/2})$, where $K^*$ is the modified equilibrium constant for volatile species. We find out that the ratio of Rb and Pb residual fraction ($f_{Rb}(melt)/f_{Pb}(melt)$) becomes large with an increasing oxygen fugacity using parameters from Sossi et al., (2019). The assumed temperature is 1400 ℃ and log$fO_2$ is -8 for melting pools. Under this condition, the cumulative fraction of Pb loss within the first 20% accretion is above 80%, meanwhile, the fraction of Rb is around 74%. Based on the content of Rb and Pb in the silicate Earth relative to CI chondrites, the loss of Pb (93%) is higher than that of Rb (74%) according to the measurement in Palme and O'Neill (2014).

We further consider the evolution of κ and μ (Figure 5). The κ value of CI chondrites (~0.92) can be used as the initial value of the solar nebula (Palme & O'Neill, 2014) and the initial μ is set to be 0.22. The κ value decreases during the condensation of the nebular dust, because of the lower condensation temperature of Rb relative to Sr. Subsequently, due to the Rb loss driven by the planetesimal-scale evaporation, the κ value continues to decline to the current value. The estimated κ of the modern BSE is 0.092 (Galimov, 2011; Carlson et al., 2015). The pre-evaporation κ value is constrained to be 0.35 by 74% Rb loss in simulations assumed a constant Sr content. However, the increasing μ is inversely related to the decreasing κ. It increases to 4-5 from the pre-evaporation value of 0.65. The final μ is expected to reach 8-10 for 93.7% Pb loss after the last large-scale U/Pb fractionation (Figure 5).

## 5. Effects on the Final Composition of Pb Isotopes

### 5.1 The Pb isotopic composition in BSE

The two U-Pb decay systems are $^{235}$U-$^{207}$Pb ($\lambda_1$=9.8485×10$^{-10}$ year$^{-1}$) and $^{238}$U-$^{206}$Pb ($\lambda_2$=1.55125×10$^{-10}$ year$^{-1}$). The formulas of isochrons for two systems are expressed in terms of μ: $(^{207}Pb/^{204}Pb)_{today} = (^{207}Pb/^{204}Pb)_{i} + \mu_{today}/137.786 * (e^{\lambda_1 t} - 1)$ and $(^{206}Pb/^{204}Pb)_{today} = (^{206}Pb/^{204}Pb)_{i} + \mu_{today} * (e^{\lambda_2 t} - 1)$, in which 'i' represents the initial value and 'today' represents the current value. The initial values of Pb isotopic composition in the early Solar System are the measured values of troilite without uranium in the IAB iron meteorite from Canyon Diablo. $(^{206}Pb/^{204}Pb)_{i} = 9.307$ and $(^{207}Pb/^{204}Pb)_{i}$=10.294 (Tatsumoto et al., 1973). The isochron of $^{207}$Pb-$^{206}$Pb is expressed as $\left((^{207}Pb/^{204}Pb)_{today} - (^{207}Pb/^{204}Pb)_{i}\right) / \left((^{206}Pb/^{204}Pb)_{today} - (^{206}Pb/^{204}Pb)_{i}\right) = 1/137.786 * \left(e^{\lambda_1 t} - 1\right)/\left(e^{\lambda_2 t} - 1\right)$ (Connelly et al., 2017). The above formula shows that the slope of $^{207}$Pb-$^{206}$Pb isochron is not associated with the μ value and it is positively correlated with time.

The Pb isotopic composition in the bulk silicate Earth mainly derives from Pb isotope data of oceanic basalts in the PetDb Database (www.earthchem.org/petdb). The proportion of MORB and OIB in the oceanic basalts is about 93.75% and 6.25% (Crisp, 1984; Gale et al., 2013). The data of global MORB is from Stracke et al. (2005) in the PetDb database (www.earthchem.org/petdb), and that of OIB is from Tuvalu, Hawaii, and Baffin (Finlayson et al., 2018; DeFelice et al., 2019; Willhite et al., 2019). Generally, the OIB values are more scattered and the average value is higher than the MORB value (Figure 6). The weighted average values of Pb isotopic compositions in modern BSE are $(^{206}Pb/^{204}Pb)_{today} = 18.462$ and $(^{207}Pb/^{204}Pb)_{today} = 15.508$ (Figure 6). The range of $^{206}$Pb/$^{204}$Pb value is from 16.58 to 21.65 and $^{207}$Pb/$^{204}$Pb value is from 15.29 to 15.80.

The global distribution of $^{206}Pb/^{204}Pb$ and $^{207}Pb/^{204}Pb$ deviates right to the 4.567-Ga (billion years) isochron of the Earth (Figure 6), which is known as the first terrestrial Pb paradox. The 4.567 Ga is regarded as the age of the Solar System by U-Pb dating of the oldest solids, calcium aluminum inclusions (CAIs) (Amelin et al., 2010).

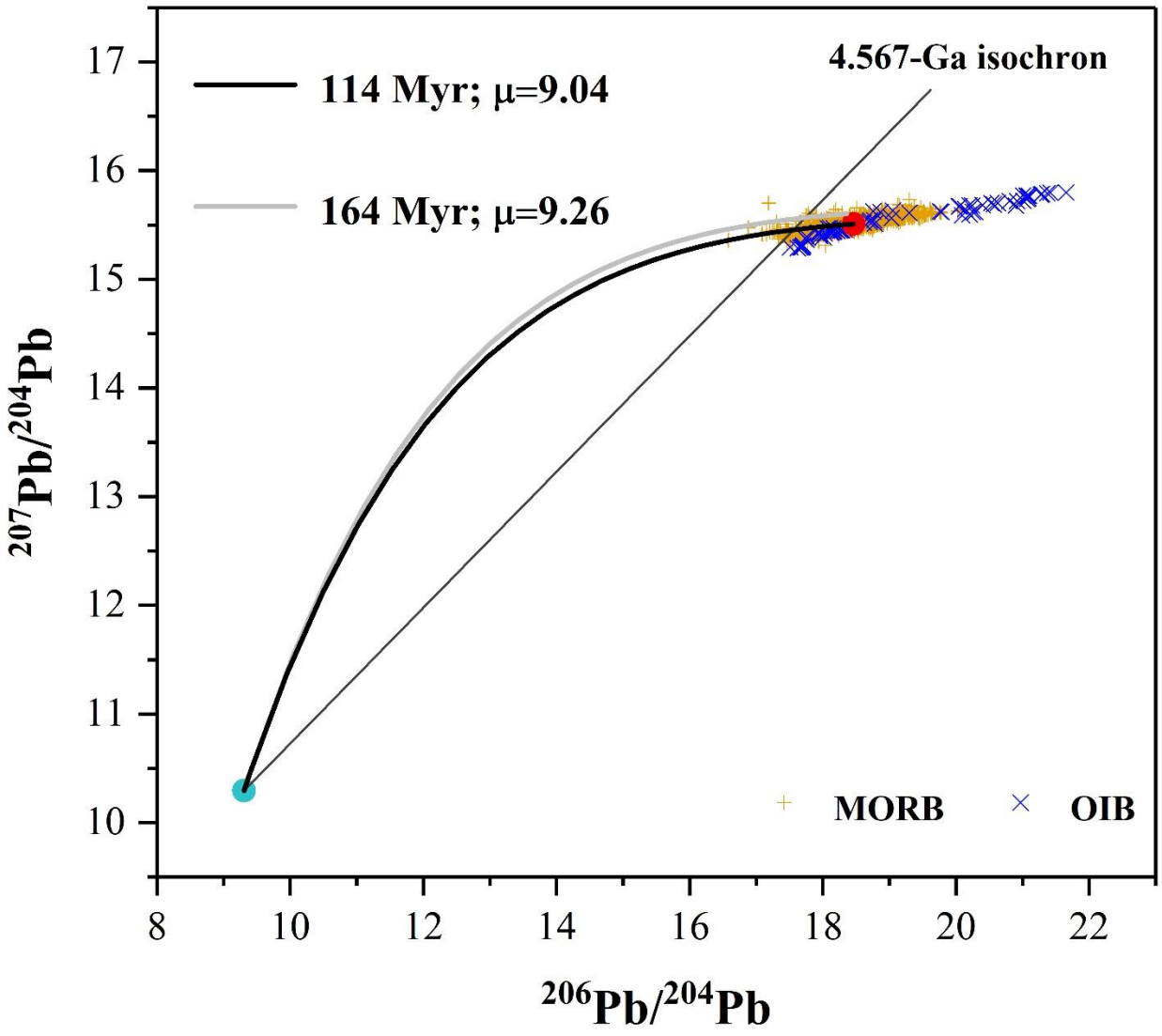


**Figure 6.** The diagram of Pb isotopes ($^{206}Pb/^{204}Pb$-$^{207}Pb/^{204}Pb$). The initial Pb isotopic composition is from Tatsumoto et al. (1973), that is $(^{206}Pb/^{204}Pb)_i$ = 9.307 and $(^{207}Pb/^{204}Pb)_i$ = 10.294. For the modern oceanic basalts including mid-ocean ridge basalts (MORB) and oceanic island basalts (OIB), the weighted average value of $^{206}Pb/^{204}Pb$ is 18.462 and $^{207}Pb/^{204}Pb$ is 15.508. The Pb isotopic data is

derived from the PetDb Database (www.earthchem.org/petdb). Growing curves evolve from an initial μ value of 0.22 in the two-stage model with the evaporation within 3 Myr. The last large-scale U/Pb fractionation is constrained to be 114 Myr with an evolved μ value of 9.04 shown as the black line and to be 164 Myr with an evolved μ value of 9.26 shown as the grey line.

5.2 The evolution of Pb isotopic composition with μ bursts

The evolution of $^{207}Pb/^{204}Pb$ and $^{206}Pb/^{204}Pb$ from the beginning of the proto-Earth to the present is a multi-stage process, in which the μ value in the silicate part increases episodically. Therefore, the formula of the evolved Pb isotopes can be divided by time according to the different μ values. From the beginning of the multi-stage accretion to the present BSE, at various time $t_0 \rightarrow t_1 \rightarrow t_2 \rightarrow \ldots\ldots t_{n-1} \rightarrow t_n \rightarrow t_{today}$, the evolution of $^{206}Pb/^{204}Pb$ is:

$$\left(\frac{^{206}Pb}{^{204}Pb}\right)_{t_n} = \left(\frac{^{206}Pb}{^{204}Pb}\right)_{t_{n-1}} + \mu_n\left(e^{\lambda_2(4.567-t_{n-1})} - e^{\lambda_2(4.567-t_n)}\right)$$

The $^{207}Pb/^{204}Pb$ ratio evolves similarly to $^{206}Pb/^{204}Pb$. Radiogenic Pb isotopes accumulate with time and the values of $^{206}Pb/^{204}Pb$ and $^{207}Pb/^{204}Pb$ increase rapidly as the μ value increases. The rapid growth of μ value in the first 3 Myr is induced by Pb evaporation during the first 20% Earth accretion. The subsequent increase of μ possibly caused by a late large-scale U/Pb fractionation can explain the excess of radiogenic Pb isotopes in BSE (Savage et al., 2015; Connelly & Bizzarro, 2016). By calculating the proper μ and the time of fractionation (see below), the evolved $^{206}Pb/^{204}Pb$ and $^{207}Pb/^{204}Pb$ can match the current values within errors. Figure 6 shows two cases of the two-stage model with early evaporation in one N-body simulation and different late fractionations. The initial μ is set to be 0.22 and increase to 1.51 within 3 Myr. In the first case, the μ value after the fractionation is about 9.26 and the proper time of fractionation is about 164 Myr. The evolved $^{206}Pb/^{204}Pb$ and $^{207}Pb/^{204}Pb$ can perfectly match the average values in BSE. In the other case, the evolved Pb isotopic

354 composition has a slight deviation from the current value and its μ value increases to 9.04 at 114 Myr
355 (Figure 6). Therefore, this model can reasonably explain the Pb paradox.

356 **6. Constraints on the Time of the Last U/Pb Fractionation Event**

357 We show in Section 3.4 that the planetesimal-scale Pb evaporation cannot satisfy the total Pb
358 loss and μ value of the modern BSE. Further Pb loss is probably caused by the multi-stage core
359 segregation or a late giant fractionation event. The two-stage model driven by a late U/Pb
360 fractionation can effectively explain the deviation of Pb isotopic composition in the silicate Earth to
361 the right of the Earth isochron (Savage et al., 2015; Connelly & Bizzarro, 2016), also seen in Figure
362 6. However, the multi-stage core segregation makes little contribution to this deviation. A late global
363 U/Pb fractionation event could be a Moon-forming giant impact or segregation of the iron sulfide
364 melting termed as "Hadean matte" during the late accretion of the Earth (Savage et al., 2015;
365 Connelly & Bizzarro, 2016; Rubie et al., 2016).

366 Connelly and Bizzarro (2016) gives a young age constraint of 4.426-4.417 Ga on the
367 Moon-forming giant impact with a traditional two-stage Pb evolution model. The small variation of
368 $^{206}Pb/^{204}Pb$ and $^{207}Pb/^{204}Pb$ in BSE results in a strong constraint on the coupled μ value and the time
369 of the last U/Pb fractionation (Figure 7). In the traditional two-stage model, we set an initial μ value
370 of 0.22 and μ increases to 8-10 after the last large-scale fractionation. When limiting the evolved Pb
371 isotopic component to the current value, the post-fractionation μ value is 9.26 on average and the
372 time of the fractionation is 140 Myr from the beginning of the Solar System (Figure 7). Considering
373 the early evaporation of Pb, more than 80% Pb diffuses into space within the first 3 Myr. The μ value
374 varies from 0.22 to 1.51 or from 0.6 to 4.12. Then the timing of the fractionation can be postponed to
375 165 Myr or 240 Myr on average (Figure 7). When the last U/Pb fractionation event is the

Moon-formation giant impact, our model can greatly postpone the timing of Moon formation and provide a young age, 165-240 Myr. Two age ranges for the Moon have been discussed in Maltese and Mazger (2020), 30-160 Myr or 200-230 Myr from the beginning of the Solar System. The estimated age for the Moon in our model is consistent with the latter.

**a.**

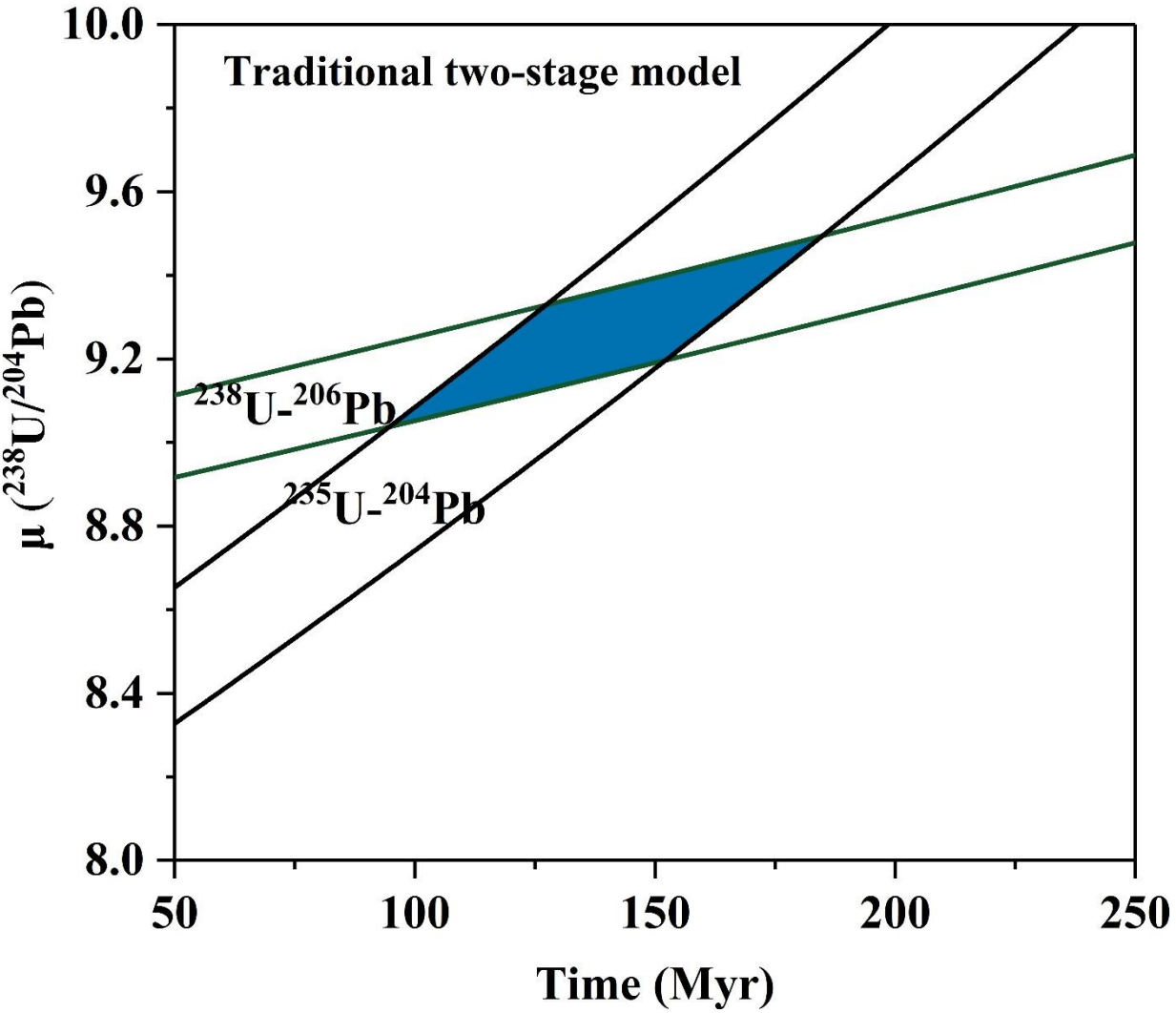

383 **b.**

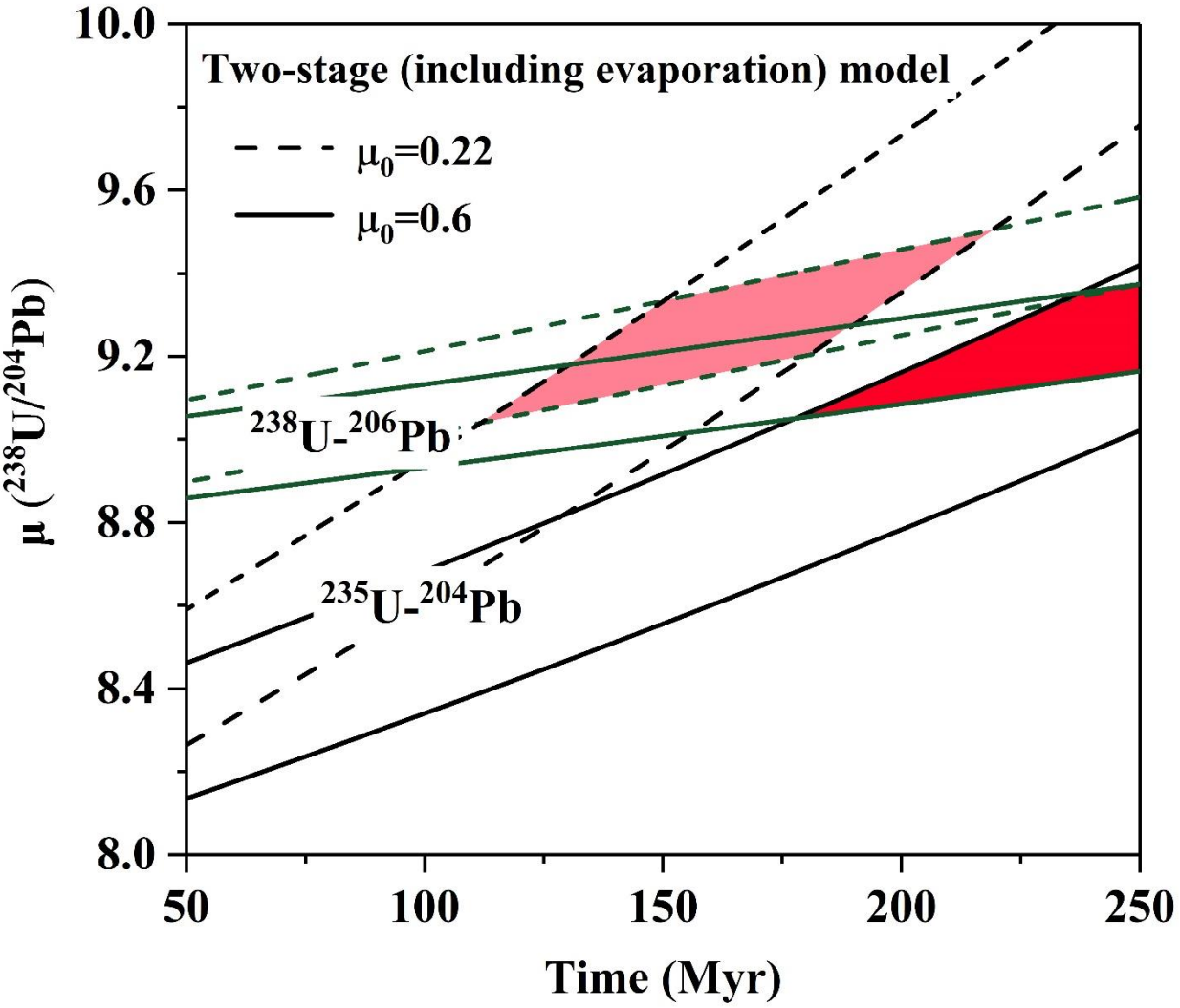


384

385 **Figure 7.** Constraints from the $^{238}$U-$^{206}$Pb and $^{235}$U-$^{207}$Pb systems on the μ value and the time of the
386 last large-scale fractionation. The shaded areas represent the proper range of the pairs of μ and time
387 of the final U/Pb fractionation to match the current Pb isotopic composition. The final $^{206}$Pb/$^{204}$Pb is
388 set to be 18.462±0.1 and the final $^{207}$Pb/$^{204}$Pb is set to be 15.508±0.1. **a.** the traditional two-stage
389 model from an initial μ value of 0.22 to the final value of 8-10. **b.** the two-stage model with the early
390 planetesimal-scale evaporation from an initial value of 0.22 (dashed line and light red area) or from
391 an initial value of 0.6 (solid line and dark red area).

392 However, the oldest age of lunar samples from the U-Pb dating of zircon is 4.417Ga (Nemchin

et al., 2009), which is a lower limit of the solidification timing of the lunar magma ocean. Therefore, the last U/Pb fractionation obtained in our model occurs after the Moon formation. The segregation of Hadean matte in the late accretion (later than the Moon-forming giant impact and before 3.8 Ga) drives the second extraction of the chalcophile elements, e.g., Pb into the metal core or to the core-mantle boundary (O'Neill et al., 1991). This causes the last global U/Pb fractionation, resulting in the final increase of μ. In our model, the timing of the Hadean matte event is limited to 165 Myr with a pre-fractionation μ of 1.51 or to 240 Myr with a pre-fractionation μ of 4.12. 55%-84% of Pb is removed from the bulk silicate Earth in this process.

## 7. Conclusions

The planetesimal-scaled evaporation induced by the collisional melting has a critical effect on the content of the moderately volatile element, e.g., Pb. It is the main factor of the Pb loss in BSE rather than the hidden Pb reservoir and the separation of the core. The episodic increment of U/Pb ratio (μ) causes a multi-stage evolution of U-Pb isotopic composition within the first 3 million years. Besides, a further two-stage model driven by a late large-scale U/Pb fractionation is required for the additional increase of μ and the excess of the radiogenic Pb isotopes.

1. The collisions between planetesimals produce magma pools or magma oceans on the targets. For targets smaller than 0.2 $M_e$, volatiles e.g., Pb can easily dissipate into space at the surface of magma pools. The N-body simulations provide the collisional parameters to calculate the volume and depth of the melt and the melting fraction. As a result, the melting mass generally increases with the accreting mass of the target (within 0.2 $M_e$) as well as the Pb evaporation.

2. In the first 20% accretion of proto-Earth, the cumulative Pb loss is 80%-90% to the maximum. Pb mostly evaporates as sulfides (PbS) and evaporates from the silicate melt as PbO(g) and Pb(g). The

fraction of Pb loss as sulfides decreases with sulfur loss. Pb loss fraction in the silicate melt is controlled by the temperature and oxygen fugacity. High-T and reduced condition promotes the huge amount of Pb evaporation.

3. $^{238}U/^{204}Pb$ referred to μ is inversely correlated with Pb loss. When the initial μ value of planetesimals is set to be 0.22-0.6, the μ value of the proto-Earth can increase to 1.5-4 in the multi-stage accretion within 3 Myr. This is not consistent with the measured value of modern BSE (8-10). Therefore, a subsequent Pb loss in a late U/Pb fractionation event is required.

4. The values of $^{87}Rb/^{86}Sr$ (κ) and $^{238}U/^{204}Pb$ (μ) in various geological bodies have a generally inverse correlation, which confirms the critical effect of the early Pb and Rb evaporation events. Because Pb is more volatile than Rb and Pb shows sulfur affinity or iron affinity, the increment of the μ (0.22-9.26) is greater than the decrement of the κ (0.92-0.09).

5. For the U-Pb decay system, a late large-scale U/Pb fractionation or a huge increase of μ can produce an excess of the radiogenic Pb isotopes. In the traditional model without the early evaporation, a fractionation at 140 Myr resulting in an average μ value of 9.26 can effectively explain “the first Pb paradox”. When considering the early Pb evaporation, the proper timing of fractionation is postponed to 165 Myr for μ from 0.22 and to 240 Myr for μ from 0.6.

6. Although the age range (165-240 Myr) of our model satisfies a group of young ages of Moon formation, it exceeds the lower limit for the solidification time of the lunar magma ocean (4.417 Ga). Therefore, the last U/Pb fractionation possibly represents the “Hadean matte” event after the Moon-forming giant impact. In conclusion, global segregation of iron sulfide melt carrying 55%-84% Pb into the core at 165-240 Myr, which causes an excess of radiogenic Pb isotopes in BSE.

**Acknowledgements**

Thanks for the calculation resources from Liu Yun group (Institute of Geochemistry, Guiyang). Thanks to the coworkers for the technical support and the spur on my scientific research. This work is supported by the Taishan Scholar Program of Shandong (ts201712075) and AoShan Talents Program Supported by Qingdao National Laboratory for Marine Science and Technology (2017ASTCP-OS07).

**Data Availability Statement**

The dataset contents the results of N-body simulations and the calculations for the U-Pb system in this study, which is uploading to 4TU. ResearchData repository (at a preparing doi: http://doi.org/10.4121/13561979). A private link is available for preview (https://figshare.com/s/9ba6513ac5bebcaff543).

## References


Abramov, O., Wong, S.M., & Kring, D.A. (2012). Differential melt scaling for oblique impacts on terrestrial planets. *Icarus*, *218*(2), 906-916. https://doi.org/10.1016/j.icarus.2011.12.022

Albarède, F. (2009). Volatile accretion history of the terrestrial planets and dynamic implications. *Nature*, *461*, 1227-1233. https://doi.org/10.1038/nature08477

Albarède, F., Albalat, E., & Lee, C.T.A. (2015). An intrinsic volatility scale relevant to the Earth and Moon and the status of water in the Moon. *Meteoritics & Planetary Science*, *50*(4), 568-577, https://doi.org/10.1111/maps.12331

Allègre, C.J., Poirier, J.P., Humler, E., & Hofmann, A.W. (1995). The chemical-composition of the Earth. *Earth and Planetary Science Letters*, *134*(3-4), 515-526. https://doi.org/10.1016/0012-821x(95)00123-t

Amelin, Y., Kaltenbach, A., Iizuka, T., Stirling, C.H., Ireland, T.R., Petaev, M., & Jacobsen, S.B. (2010). U-Pb chronology of the Solar System's oldest solids with variable U-238/U-235. *Earth and Planetary Science Letters*, *300*(3-4), 343-350. https://doi.org/10.1016/j.epsl.2010.10.015

Anders, E., & Grevesse, N. (1989). Abundances of the Elements - Meteoritic and Solar. *Geochimica Et Cosmochimica Acta*, *53*(1), 197-214. https://doi.org/10.1016/0016-7037(89)90286-X

Ballhaus, C., Laurenz, V., Munker, C., Fonseca, R.O.C., Albarede, F., Rohrbach, A., et al. (2013). The U/Pb ratio of the Earth's mantle-A signature of late volatile addition. *Earth and Planetary Science Letters*, *362*, 237-245. https://doi.org/10.1016/j.epsl.2012.11.049

Barr, A.C., & Citron, R.I. (2011). Scaling of melt production in hypervelocity impacts from high-resolution numerical simulations. *Icarus*, *211*(1), 913-916. https://doi.org/10.1016/j.icarus.2010.10.022

469 Benedikt, M.R., Scherf, M., Lammer, H., Marcq, E., Odert, P., Leitzinger, M., & Erkaev, N.V. (2020).
470 Escape of rock-forming volatile elements and noble gases from planetary embryos. *Icarus*, *347*,
471 https://doi.org/10.1016/j.icarus.2020.113772
472 Bjorkman, M.D., & Holsapple, K.A. (1987). Velocity scaling impact melt volume. *International*
473 *Journal of Impact Engineering*, *5*, 155-163. https://doi.org/10.1016/0734-743X(87)90035-2
474 Borg, L.E., Edmunson, J.E., & Asmerom, Y. (2005). Constraints on the U-Pb isotopic systematics of
475 Mars inferred from a combined U-Pb, Rb-Sr, and Sm-Nd isotopic study of the Martian meteorite
476 Zagami. *Geochimica Et Cosmochimica Acta*, *69*(24), 5819-5830.
477 https://doi.org/10.1016/j.gca.2005.08.007
478 Bouhifd, M.A., Andrault, D., Bolfan-Casanova, N., Hammouda, T., & Devidal, J.L. (2013).
479 Metal-silicate partitioning of Pb and U: Effects of metal composition and oxygen fugacity.
480 *Geochimica Et Cosmochimica Acta*, *114*, 13-28. https://doi.org/10.1016/j.gca.2013.03.034
481 Bouvier, A., Blichert-Toft, J., & Albarede, F. (2009). Martian meteorite chronology and the evolution
482 of the interior of Mars. *Earth and Planetary Science Letters*, *280*(1-4), 285-295.
483 https://doi.org/10.1016/j.epsl.2009.01.042
484 Bouvier, A., Blichert-Toft, J., Vervoort, J.D., & Albarede, F. (2005). The age of SNC meteorites and
485 the antiquity of the Martian surface. *Earth and Planetary Science Letters*, *240*(2), 221-233.
486 https://doi.org/10.1016/j.epsl.2005.09.007
487 Burton, K.W., Cenki-Tok, B., Mokadem, F., Harvey, J., Gannoun, A., Alard, O., & Parkinson, I.J.
488 (2012). Unradiogenic lead in Earth’s upper mantle. *Nature Geoscience*, *5*, 570.
489 https://doi.org/10.1038/ngeo1531
490 Canup, R.M., & Asphaug, E. (2001). Origin of the Moon in a giant impact near the end of the Earth's

491 formation. *Nature*, *412*, 708-712. https://doi.org/10.1038/35089010
492 Carlson, R.W., Boyet, M., O'Neill, J., Rizo, H., & Wade, R.J. (2015). Early differentiation and its
493 long-term consequences for Earth evolution, in J. Badro & M.J. Walter (Eds.), *The Early Earth:*
494 *Accretion and Differentiation*, *Geophysical Monograph Series*, (pp. 143-172). Washington, DC:
495 American Geophysical Union. https://doi.org/10.1002/9781118860359.ch8
496 Carter, P.J., Leinhardt, Z.M., Elliott, T., Walter, M.J., & Stewart, S.T. (2015). Compositional
497 evolution during rocky protoplanet accretion. *Astrophysical Journal*, *813*(1), 72.
498 https://doi.org/10.1088/0004-637X/813/1/72
499 Chambers, J.E. (1999). A hybrid symplectic integrator that permits close encounters between massive
500 bodies. *Monthly Notices Of The Royal Astronomical Society*, *304*(4), 793-799.
501 https://doi.org/10.1046/j.1365-8711.1999.02379.x
502 Chambers, J.E. (2004). Planetary accretion in the inner Solar System. *Earth and Planetary Science*
503 *Letters*, *223*(3-4), 241-252. https://doi.org/10.1016/j.epsl.2004.04.031
504 Connelly, J.N., & Bizzarro, M. (2016). Lead isotope evidence for a young formation age of the
505 Earth-Moon system. *Earth and Planetary Science Letters*, *452*, 36-43.
506 https://doi.org/10.1016/j.epsl.2016.07.010
507 Connelly, J.N., Bollard, J., & Bizzarro, M. (2017). Pb-Pb chronometry and the early Solar System.
508 *Geochimica Et Cosmochimica Acta*, *201*, 345-363. https://doi.org/10.1016/j.gca.2016.10.044
509 Crisp, J.A. (1984). Rates of magma emplacement and volcanic output. *Journal of Volcanology and*
510 *Geothermal Research*, *20*(3-4), 177-211. https://doi.org/10.1016/0377-0273(84)90039-8
511 Dauphas, N., Poitrasson, F., Burkhardt, C., Kobayashi, H., & Kurosawa, K. (2015). Planetary and
512 meteoritic Mg/Si and delta Si-30 variations inherited from solar nebula chemistry. *Earth and*

513 *Planetary Science Letters*, *427*, 236-248. https://doi.org/10.1016/j.epsl.2015.07.008
514 Davies, E.J., Carter, P.J., Root, S., Kraus, R.G., Spaulding, D.K., Stewart, S.T., & Jacobsen, S.B.
515 (2020). Silicate melting and vaporization during rocky planet formation. *Journal of Geophysical*
516 *Research-Planets*, *125*(2). https://doi.org/10.1029/2019JE006227
517 DeFelice, C., Mallick, S., Saal, A.E., & Huang, S. (2019). An isotopically depleted lower mantle
518 component is intrinsic to the Hawaiian mantle plume. *Nature Geoscience*, *12*(6), 1-6.
519 https://doi.org/10.1038/s41561-019-0348-0
520 Deng, H.P., Ballmer, M.D., Reinhardt, C., Meier, M.M.M., Mayer, L., Stadel, J., & Benitez, F. (2019).
521 Primodial Earth mantle heterogeneity caused by the Moon-forming giant impact? *The Astrophysical*
522 *Journal*, *887*(2). https://doi.org/10.3847/1538-4357/ab50b9
523 de Vries, J., Nimmo, F., Melosh, H.J., Jacobson, S.A., Morbidelli, A., & Rubie, D.C. (2016).
524 Impact-induced melting during accretion of the Earth. *Progress in Earth and Planetary Science*, *3*.
525 https://doi.org/10.1186/s40645-016-0083-8
526 Elkins-Tanton, L.T. (2012). Magma oceans in the inner Solar System. *Annual Review of Earth and*
527 *Planetary Sciences*, *40*, 113-139. https://doi.org/10.1146/annurev-earth-042711-105503
528 Fang, T., & Deng, H.P. (2020). Extreme close encounters between proto-Mercury and proto-Venus
529 in terrestrial planet formation. *Monthly Notices Of The Royal Astronomical Society*, *496*(3),
530 3781-3785. https://doi.org/10.1093/mnras/staa1785
531 Finlayson, V.A., Konter, J.G., Konrad, K., Koppers, A.A.P., Jackson, M.G., & Rooney, T.O. (2018).
532 Sr-Pb-Nd-Hf isotopes and Ar-40/Ar-39 ages reveal a Hawaii-Emperor-style bend in the Rurutu
533 hotspot. *Earth and Planetary Science Letters*, *500*, 168-179.
534 https://doi.org/10.1016/j.epsl.2018.08.020

Fischer, R.A., & Ciesla, F.J. (2014). Dynamics of the terrestrial planets from a large number of N-body simulations. *Earth and Planetary Science Letters*, *392*, 28-38. https://doi.org/10.1016/j.epsl.2014.02.011

Gaffney, A.M., Borg, L.E., & Connelly, J.N. (2007). Uranium-lead isotope systematics of Mars inferred from the basaltic shergottite QUE 94201. *Geochimica Et Cosmochimica Acta*, *71*(20), 5016-5031. https://doi.org/10.1016/j.gca.2007.08.009

Gale, A., Dalton, C.A., Langmuir, C.H., Su, Y.J., & Schilling, J.G. (2013). The mean composition of ocean ridge basalts. *Geochemistry Geophysics Geosystems*, *14*(3), 489-518. https://doi.org/10.1029/2012gc004334

Galimov, E.M. (2011). Formation of the Moon and the Earth from a common supraplanetary gas-dust cloud (lecture presented at the XIX all-Russia symposium on isotope geochemistry on November 16, 2010). *Geochemistry International*, *49*(6), 537-554. https://doi.org/10.1134/S0016702911060048

Galimov, E.M. (2019). Geochemical features of the Moon and Earth predetermined by the mechanism of formation of the Earth-Moon system. *Geochemistry International*, *57*(10), 1124-1124. https://doi.org/10.1134/S0016702919100100

Halliday, A.N. (2004). Mixing, volatile loss and compositional change during impact-driven accretion of the Earth. *Nature*, *427*(6974), 505-509. https://doi.org/10.1038/nature02275

Hansen, B.M.S. (2009). Formation of the terrestrial planets from a narrow annulus. *Astrophysical Journal*, *703*(1), 1131-1140. https://doi.org/10.1088/0004-637x/703/1/1131

Hart, S.R., & Gaetani, G.A. (2006). Mantle Pb paradoxes: the sulfide solution. *Contributions To Mineralogy and Petrology*, *152*(3), 295-308. https://doi.org/10.1007/s00410-006-0108-1

Hin, R.C., Coath, C.D., Carter, P.J., Nimmo, F., Lai, Y.J., von Strandmann, P.A.E.P., et al. (2017). Magnesium isotope evidence that accretional vapour loss shapes planetary compositions. *Nature*, *549*(7673), 511-515. https://doi.org/10.1038/nature23899

Hofmann A.W. (2007). Sampling mantle heterogeneity through oceanic basalts: Isotopes and trace elements. In K. Turekian & H. Holland (Eds.), *Treatise on Geochemistry 2nd Edition, Reference Module in Earth Systems and Environmental Sciences* (Vol. 3, pp. 67-101). United Kingdon: Elsevier Science. https://doi.org/10.1016/B0-08-043751-6/02123-X

Johansen, A., Oishi, J.S., Mac Low, M.M., Klahr, H., & Henning, T. (2007). Rapid planetesimal formation in turbulent circumstellar disks. *Nature, 448*(7157), 1022-1025. https://doi.org/10.1038/nature06086

Lodders, K. (2003). Solar system abundances and condensation temperatures of the elements. *Astrophysical Journal, 591*(2), 1220-1247. https://doi.org/10.1086/375492

Malavergne, V., Tarrida, M., Combes, R., Bureau, H., Jones, J., & Schwandt, C. (2007). New high-pressure and high-temperature metal/silicate partitioning of U and Pb: Implications for the cores of the Earth and Mars. *Geochimica Et Cosmochimica Acta, 71*(10), 2637-2655. https://doi.org/10.1016/j.gca.2007.03.011

Malaviarachchi, S.P.K., Makishima, A., Tanimoto, M., Kuritani, T., & Nakamura, E. (2008). Highly unradiogenic lead isotope ratios from the Horoman peridotite in Japan. *Nature Geoscience*, *1*, 859. https://doi.org/10.1038/ngeo363

Maltese, A., & Mezger, K. (2020). The Pb isotope evolution of Bulk Silicate Earth: Constraints from its accretion and early differentiation history. *Geochimica Et Cosmochimica Acta*, *271*, 179-193. https://doi.org/10.1016/j.gca.2019.12.021

McDonough, W.F., & Sun, S.S. (1995). The composition of the Earth. *Chemical Geology*, *120*(3-4), 223-253. https://doi.org/10.1016/0009-2541(94)00140-4

Murphy, D.T., Kamber, B.S., & Collerson, K.D. (2003). A refined solution to the first terrestrial Pb-isotope paradox. *Journal Of Petrology*, *44*(1), 39-53. https://doi.org/10.1093/petrology/44.1.39

Nemchin, A., Timms, N., Pidgeon, R., Geisler, T., Reddy, S., & Meyer, C. (2009). Timing of crystallization of the lunar magma ocean constrained by the oldest zircon. *Nature Geoscience*, *2*(2), 133-136. https://doi.org/10.1038/Ngeo417

Newsom, H.E. (1995). Composition of the Solar System, planets, meteorites, and major terrestrial reservoirs. In T.J. Ahrens (Eds.), *Global Earth Physics: A Handbook of Physical Constants*, *AGU Reference Shelf*, (Vol. 1, pp. 159–189). Washington, DC: American Geophysical Union. https://doi.org/10.1029/RF001p0159

Norman, M.D., & Mittlefehldt, D.W. (2002). Impact processing of chondritic planetesimals: Siderophile and volatile element fractionation in the Chico L chondrite. *Meteoritics & Planetary Science*, *37*(3), 329-344. https://doi.org/10.1111/j.1945-5100.2002.tb00820.x

Norris, C.A., & Wood, B.J. (2017). Earth's volatile contents established by melting and vaporization. *Nature*, *549*(7673), 507-510. https://doi.org/10.1038/nature23645

O'Neill, H.St.C. (1991). The origin of the moon and the early history of the earth - A chemical model. Part 2: The earth. *Geochimica Et Cosmochimica Acta*, *55*(4), 1159-1172. https://doi.org/10.1016/0016-7037(91)90169-6

Palme, H., & O'Neill, H. (2014). Cosmochemical estimates of mantle composition. In K. Turekian & H. Holland (Eds.), *Treatise on Geochemistry 2nd Edition*, *Reference Module in Earth Systems and Environmental Sciences* (Vol. 3, pp. 1-39). United Kingdon: Elsevier Science.

https://doi.org/10.1016/B978-0-08-095975-7.00201-1

Premo, W.R., Tatsumoto, M., Misawa, K., Nakamura, N., & Kita, N.I. (1999). Pb-isotopic systematics of lunar highland rocks (> 3.9 Ga): Constraints on early lunar evolution. *International Geology Review*, *41*(2), 95-128. https://doi.org/10.1080/00206819909465134

Rubie, D.C., Laurenz, V., Jacobson, S.A., Morbidelli, A., Palme, H., Vogel, A.K., & Frost, D.J. (2016). Highly siderophile elements were stripped from Earth's mantle by iron sulfide segregation. *Science*, *353*(6304), 1141-1144. https://doi.org/10.1126/science.aaf6919

Savage, P.S., Moynier, F., Chen, H., Shofner, G., Siebert, J., Badro, J., & Puchtel, I.S. (2015) Copper isotope evidence for large-scale sulphide fractionation during Earth's differentiation. *Geochemical Perspectives Letters*, *1*(1), 53-63. https://doi.org/10.7185/geochemlet.1506

Scott, E.R.D. (2007). Chondrites and the protoplanetary disk. *Annual Review Of Earth and Planetary Sciences*, *35*, 577-620. https://doi.org/10.1146/annurev.earth.35.031306.140100

Sossi, P.A., Klemme, S., O'Neill, H.S., Berndt, J., & Moynier, F. (2019). Evaporation of moderately volatile elements from silicate melts: experiments and theory. *Geochimica Et Cosmochimica Acta*, *260*, 204-231. https://doi.org/10.1016/j.gca.2019.06.021

Stracke, A., Hofmann, A.W., & Hart, S.R. (2005). FOZO, HIMU, and the rest of the mantle zoo. *Geochemistry Geophysics Geosystems*, *6*(5). https://doi.org/10.1029/2004gc000824

Tatsumoto, M., Knight, R.J., & Allègre, C.J. (1973). Time differences in formation of meteorites as determined from ratio of Pb-207 to Pb-206. *Science*, *180*(4092), 1279-1283. https://doi.org/10.1126/science.180.4092.1279

Willhite, L.N., Jackson, M.G., Blichert-Toft, J., Bindeman, I., Kurz, M.D., Halldorsson, S.A., et al. (2019). Hot and heterogenous high-He-3/He-4 components: new constraints from proto-Iceland

623 plume lavas from Baffin Island. *Geochemistry Geophysics Geosystems*, *20*(12), 5939-5967.
624 https://doi.org/10.1029/2019gc008654
625 Williams, J.P., & Cieza, L.A. (2011). Protoplanetary disks and their evolution. *Annual Review of*
626 *Astronomy and Astrophysics*, *49*, 67-117. https://doi.org/10.1146/annurev-astro-081710-102548
627 Wood, B.J., & Halliday, A.N. (2010). The lead isotopic age of the Earth can be explained by core
628 formation alone. *Nature*, *465*, 767-770. https://doi.org/10.1038/nature09072
629 Wood, B.J., Halliday, A.N., & Rehkämper, M. (2010). Volatile accretion history of the Earth. *Nature*,
630 *467*, E6-7. https://doi.org/10.1038/nature09484
631 Wood, B.J., Smythe, D.J., & Harrison, T. (2019). The condensation temperatures of the elements: A
632 reappraisal. *American Mineralogist*, *104*(6), 844-856. https://doi.org/10.2138/am-2019-6852CCBY
633 Wood, B.J., & Wade, J. (2013). Activities and volatilities of trace components in silicate melts: a
634 novel use of metal-silicate partitioning data. *Contributions To Mineralogy and Petrology*, *166*(3),
635 911-921. https://doi.org/10.1007/s00410-013-0896-z
636 Yoshizaki, T., & McDonough, W.F. (2020). The composition of Mars. *Geochimica Et Cosmochimica*
637 *Acta*, *273*, 137-162. https://doi.org/10.1016/j.gca.2020.01.011
638 Young, E.D. (2017). Evaporating planetesimals. *Nature*, *549*(7673), 461-462.
639 https://doi.org/10.1038/549461a
640 Young, E.D., Shahar, A., Nimmo, F., Schlichting, H.E., Schauble, E.A., Tang, H.,& Labidi, J. (2019).
641 Near-equilibrium isotope fractionation during planetesimal evaporation. *Icarus*, *323*, 1-15.
642 https://doi.org/10.1016/j.icarus.2019.01.012

643 **Figures**

644 **Figure 1.** The average melting mass ($M_{melt}$) driven by multiple collisions evolves with the accreted
645 mass of the targets. Data of collisional melting derives from 100 groups of N-body simulations and
646 the error bars represent the maximum and minimum of the melting mass.

647 **Figure 2.** Pb loss fraction for each impact (bars) and the cumulative Pb loss fraction (curves) in one
648 N-body simulation until the accreted mass is up to 0.2 $M_e$. The blue bar and curve represent Pb loss
649 as sulfides; the red bar and curve represent Pb loss as oxides in silicate; the black curve represents
650 the sum of cumulative Pb loss in sulfide and silicate. The content of sulfur linerly decreases with the
651 accreting mass during the first 20% accretion.

652 **Figure 3.** The accreted mass with time and the tempal evolution of the μ value during the first 20%
653 accretion for one N-body simulation. The initial μ value is set to be 0.22-0.6 respectively. The blue
654 curves show the variation of μ under 1400℃ and log$fO_2$=-8; the red curves show the variation of μ
655 under 1300℃ and log$fO_2$=-8; the yellow curves show the variation of μ under 1400℃ and log$fO_2$=-6.

656 **Figure 4.** The relation of the μ value before the last U/Pb fractionation to the cumulative Pb loss
657 fraction under three T-log$fO_2$ conditions. The results derive from 63 groups of N-body simulations.
658 The current Pb loss fraction is estimated to be 0.93 (Palme & O'Neill, 2014).

659 **Figure 5.** The relation of the variation of κ($^{87}Rb/^{86}Sr$) and μ($^{238}U/^{204}Pb$) during the terrestrial
660 accretion. The composition of CI chondrites represents the initial composition of solar nebula
661 (κ=0.92; μ=0.22) (Palme & O'Neill, 2014). The condensation of nebula dust produces small
662 undifferentiated bodies. The assumed value of planetesimals (0.005 $M_e$) is κ=0.35 and μ=0.65 before
663 evaporation. The accreted body like Mars shows κ in the range of 0.12-0.26 and μ in the range of
664 1.5-5 (Gaffney et al., 2007; Yoshizaki & McDonough, 2020). The final κ and μ values can

approximately fall in the interval of the observed values of the present Earth mantle (κ≈0.09; μ=8-10) (Galimov, 2011). The additional increase of μ is caused by a late U/Pb fractionation.

**Figure 6.** The diagram of Pb isotopes ($^{206}Pb/^{204}Pb$-$^{207}Pb/^{204}Pb$). The initial Pb isotopic composition is from Tatsumoto et al. (1973), that is $(^{206}Pb/^{204}Pb)_i$ = 9.307 and $(^{207}Pb/^{204}Pb)_i$ = 10.294. For the modern oceanic basalts including mid-ocean ridge basalts (MORB) and oceanic island basalts (OIB), the weighted average value of $^{206}Pb/^{204}Pb$ is 18.462 and $^{207}Pb/^{204}Pb$ is 15.508. These Pb isotopic data is derived from the PetDb Database (www.earthchem.org/petdb). Growing curves evolve from an initial μ value of 0.22 in the two-stage model with the evaporation within 3 Myr. The last large-scale U/Pb fractionation is constrained to be 114 Myr with an evolved μ value of 9.04 shown as the black line and to be 164 Myr with an evolved μ value of 9.26 shown as the grey line.

**Figure 7.** Constraints from the $^{238}U$-$^{206}Pb$ and $^{235}U$-$^{207}Pb$ systems on the μ value and the time of the last large-scale fractionation. The shaded areas represent the proper range of the pairs of μ and time of the final U/Pb fractionation to match the current Pb isotopic composition. The final $^{206}Pb/^{204}Pb$ is set to be 18.462±0.1 and the final $^{207}Pb/^{204}Pb$ is set to be 15.508±0.1. **a.** the traditional two-stage model from an initial μ value of 0.22 to the final value of 8-10. **b.** the two-stage model with the early planetesimal-scale evaporation from an initial value of 0.22 (dashed line and light red area) or from an initial value of 0.6 (solid line and dark red area).

## Tables

### Table 1

*The μ value in planetary reservoirs*